

**Table S1.** Parameter values for IDMatch ([www.github.com/sgindraux/IDMatch](http://www.github.com/sgindraux/IDMatch)). Here, F1 is a median filter, F2 is a histogram equalization filter and F3 is called Contrast Limited Adaptive Histogram Equalization (CLAHE) filter. The method M1 is Normalized Cross Correlation and M2 is Orientation Correlation.

Parameter	Value
Mode	1
Applied filters	F1, F2, F3, F1F2, F1F3
Pixel deviation	4
Step points	2
Number windows	5
Applied Methods	M1, M2
Times step	8
Minimum Window Members	15

## 1 SUPPLEMENTARY

### 2 Velocity validation

3 The difference between GPS and satellite velocities vary from 8 to 14% for the four stations (Fig. 1),  
 4 averaged over the period that the GPS stations were operated. For B, C and D, the GPS velocities are  
 5 higher but for station A, which is the closest to the front, the satellite-derived velocity is 12% higher.  
 6 However, the discrepancy could be attributed to the differences in measurement periods, 7 to 16 July for  
 7 the GPS and 4 to 24 July for the satellite velocity. The four-hour average TRI velocity is extracted at the  
 8 location of the four GPS stations and compared to the velocity recorded with GPS, which is also projected  
 9 along the line of sight of the TRI (Fig. S3). We find a root mean square error of 8 to 12 %, when both  
 10 GPS and TRI velocities are available.

### 11 Basal inversion

12 The inversion method (Gillet-Chaulet and others, 2012) minimizes a cost function that consists of two terms,  
 13 the cost due to misfit between modeled and observed velocities and a weighted regularization cost that  
 14 penalizes spatial derivatives of the inverted sliding coefficient to avoid over-fitting the velocity observations  
 15 and to guarantee a smooth sliding coefficient. We follow an L-curve approach (Hansen, 2001), by plotting  
 16 the smoothness of the optimized sliding coefficient as a function of the mismatch between the model and

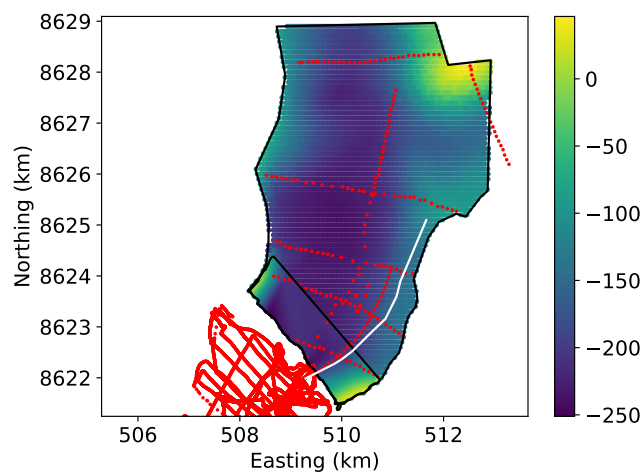


**Fig. S1.** Bedrock digital elevation model (DEM) used in the numerical simulations. The location of the measurements used for the updated bedrock DEM are shown in red and a line of highest shear is shown in white. The UTM zone 19N coordinate projection is used.

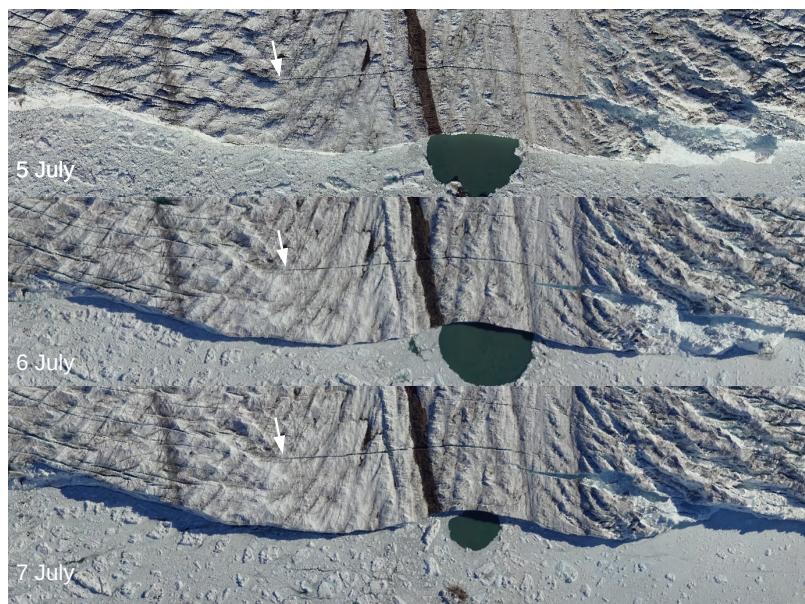


**Fig. S2.** UAV-derived ortho-images 5, 6 and 7 July 2017 prior to the calving event. A white arrow shows the position of the crevasse tip in each ortho-image.

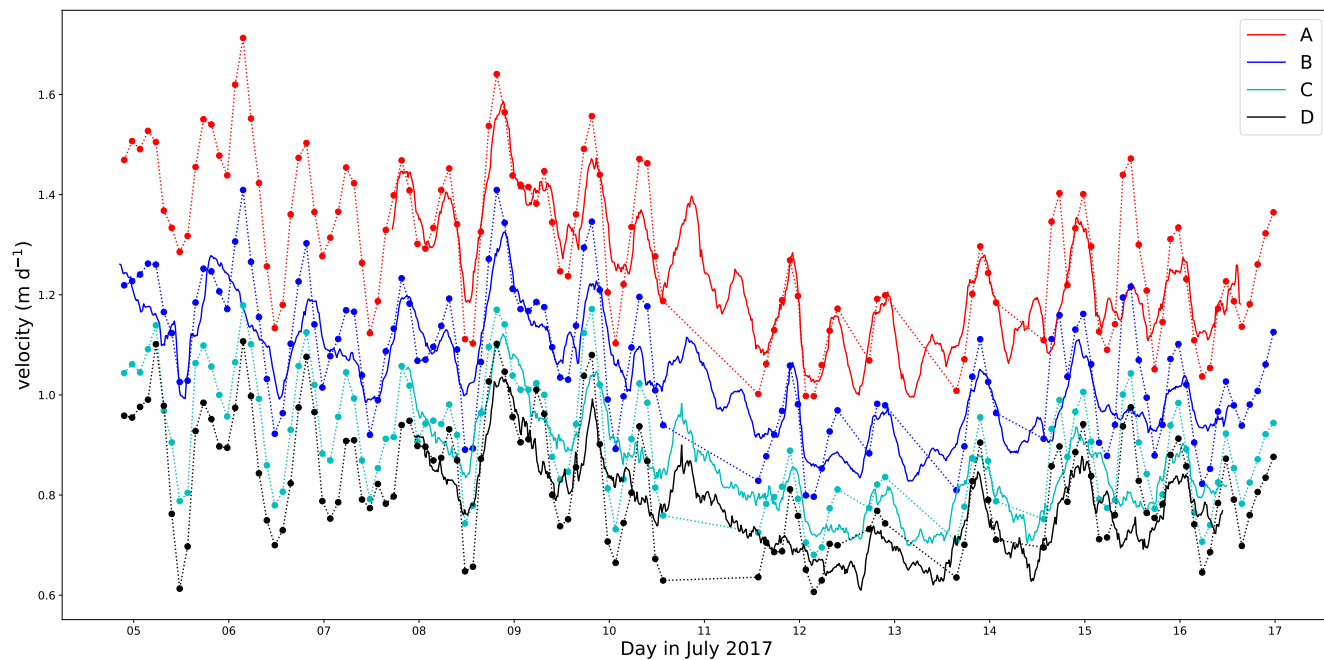


**Fig. S3.** GPS velocity calculated in four-hour window projected to the line of sight of the TRI (continuous line) in comparison to four-hour averaged TRI velocity (dotted line with large dots for data points).

17 the observations (Fig. S4) for varying regularisation weights. We find that the regularisation weight  $10^8$   
 18 compromises between a smooth sliding coefficient distribution and a small misfit for the two enhancement  
 19 factors  $E$ . The resulting velocity, sliding coefficient and misfits are shown in Figs. S5 and S6. The absolute  
 20 misfit between observed and modelled velocity is generally below  $0.3 \text{ m d}^{-1}$  (see Fig. S5c and d).

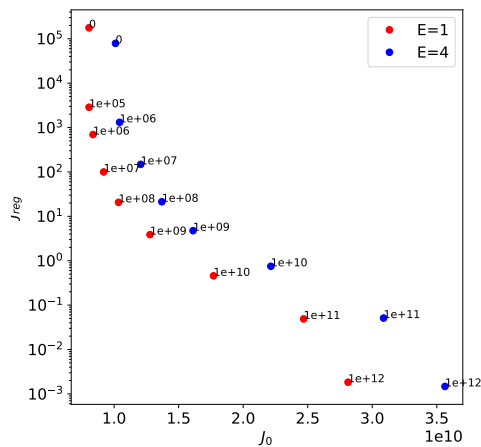


**Fig. S4.** L-curve of the inversion method obtained for  $E = 1$  and  $E = 4$ . The cost  $J_0$  is due to the mismatch between the model and the observations and  $J_{reg}$  due to spatial derivatives of the sliding coefficient  $C$ . The optimal regularisation parameter  $\lambda=10^8$  is chosen.

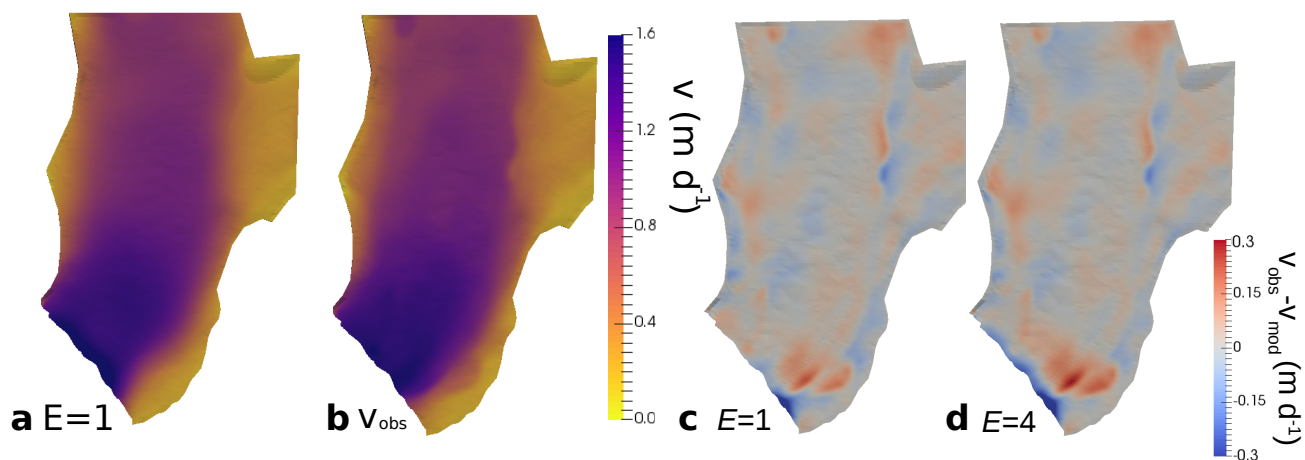


**Fig. S5.** Modeled velocity ( $\text{m d}^{-1}$ ) with the inverted friction coefficient  $C$  is shown for  $E = 1$  (a), together with the observed velocity (b) and the misfit  $v_{obs} - v_{mod}$  for both  $E$  (c and d).

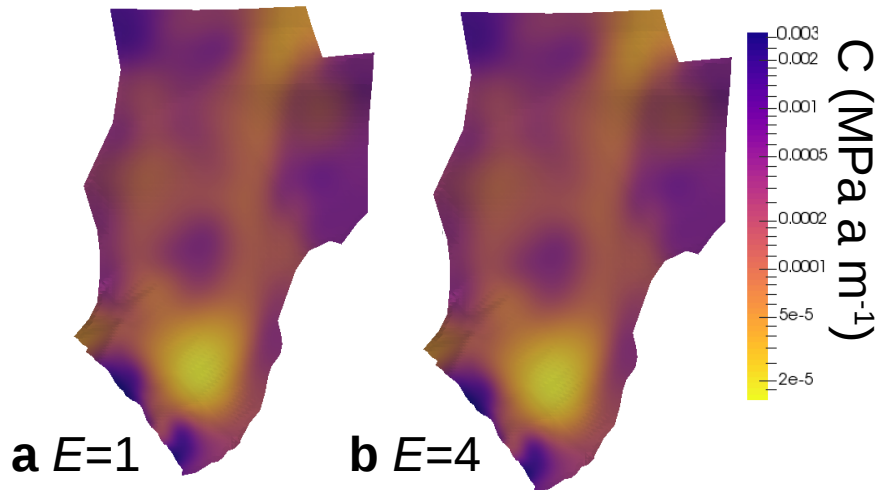


**Fig. S6.** The inverted friction coefficient  $C$  (MPa a m<sup>-1</sup>) is shown for all values  $E$  using a logarithmic scale.

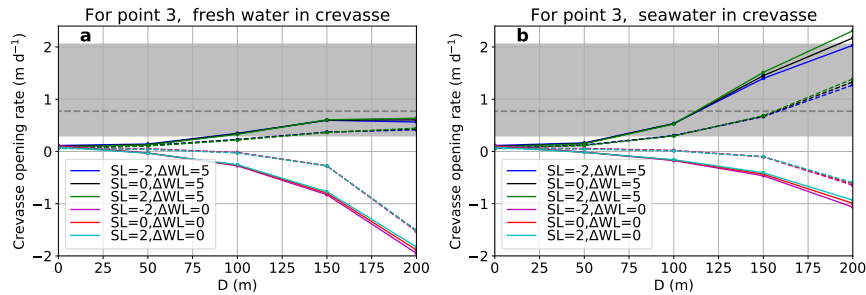


**Fig. S7.** Opening rates for varying depths, sea levels and water-level difference, in line of sight of the TRI for point 3 (Fig. 5), for a fresh-water filled crevasse (a) and for seawater (b). The coloured solid lines are for  $E = 4$  and the coloured dashed lines for  $E = 1$ . The grey area outlines the observed range and the horizontal grey dashed line is the mean of the opening rate over time.

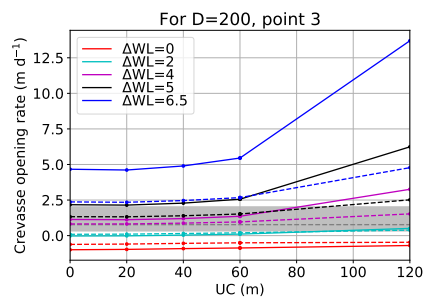


**Fig. S8.** Opening rates for varying undercut sizes ( $UC$ ) and  $D = 200$  m, in line of sight of the TRI for point 3 (Fig. 5), for a seawater-filled crevasse. The coloured continuous lines are for  $E = 4$  and the coloured dashed lines for  $E = 1$ . The grey area outlines the observed range and the grey dashed line is the mean of the opening rate over time.

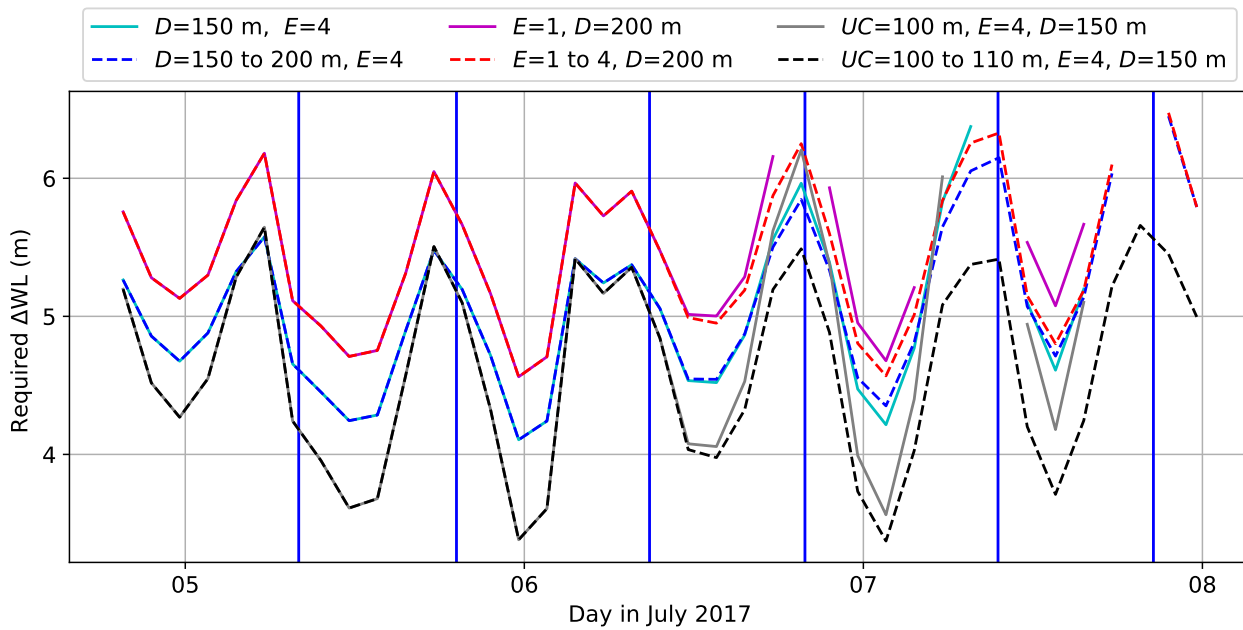


**Fig. S9.** Required water-level difference  $\Delta WL$  in order to reproduce observed opening rates for six scenarios for a crevasse filled with fresh water. The vertical blue lines show the occurrence of low tide. Gaps in the lines show where tested water levels were not sufficient to reach observed opening rates. Dashed lines show configurations where not only  $\Delta WL$  changes but also  $E$ ,  $D$  or  $UC$  changes after 36 hours. Note that some configurations require similar  $\Delta WL$ , hence lines partially overlap.

21 **REFERENCES**

- 22 Gillet-Chaulet F, Gagliardini O, Seddik H, Nodet M, Durand G, Ritz C, Zwinger T, Greve R and Vaughan DG  
23 (2012) Greenland ice sheet contribution to sea-level rise from a new-generation ice-sheet model. *Cryosphere*, **6**(6),  
24 1561–1576
- 25 Hansen P (2001) The L-curve and its use in the numerical treatment of inverse problems. computational inverse  
26 problems in electrocardiology. *Adv. Comput. Bioeng.*, **5**, 119